

The Influence of Palladium on the Structure and Catalytic Activity of Lanthanum Based Mixed Oxide

Hua Zhong^{a,b*} and Hongliang Xie^{a,b}

^aProvincial Key Laboratory of Coordination Chemistry, Jianggangshan University, Jian, 343009, People's Republic of China.

^bCollege of Chemistry and Chemical Engineering, Jianggangshan University, Jian, 343009, People's Republic of China.

Received 1 August 2008, revised 20 December 2008, accepted 10 February 2009.

ABSTRACT

LaSrCo_{0.9}Pd_{0.1}O₄ and LaSrCoO₄ mixed oxides were prepared and characterized by XRD, FTIR, BET and XPS, then studied for the reduction of NO by CO. The results show that all samples display characteristic peaks of crystal structure A₂BO₄ and show the rather strong diffraction pattern for LaSrCo_{0.9}Pd_{0.1}O₄ (reduced and oxidized) and weak signals of lanthanum oxide for LaSrCo_{0.9}Pd_{0.1}O₄ (reduced). The noble metal Pd has a significant influence on the specific surface areas, pore volumes, binding energies and activities of the samples. For NO reduction by CO, catalytic activity shows complete conversion below 360 °C and the order of activity is LaSrCo_{0.9}Pd_{0.1}O₄ (reduced and oxidized) > LaSrCo_{0.9}Pd_{0.1}O₄ (reduced) > LaSrCoO₄ (reduced). Kinetic analysis for NO reduction by CO indicates that the specific reaction rate is significantly affected by the synthesis procedure.

KEYWORDS

Noble metal Pd, NO reduction by CO, XPS.

1. Introduction

For the elimination of CO, low hydrocarbon and NO_x contaminations exhausted from motor vehicles, catalytic converters are the industry's standard technology.¹ Therefore, the reduction of NO by CO is of particular interest and has been studied by a number of researchers on various perovskite oxides, since both gases usually exist in effluent gas mixtures.^{2–5} Recently, the perovskite-type A₂BO₄ mixed oxides of K₂NiF₄ structure, consisting of alternating layers of ABO₃ perovskite^{6–8} and AO were studied as new materials for their low cost, high catalytic activity and high thermal stability.⁹ This structure type forms solid solutions with a number of cations, which enables the alteration of the physical-chemical properties over a wide range. The replacement of A- and/or B-site cations by other metal cations often brings about the formation of crystal microstrain. We have reported the investigations of CO and C₃H₈ oxidation-catalyzing reactions over LnSrBO₄ (Ln = La, Pr, Nd, Sm and Eu) catalysts.^{10–14} In addition, conventional catalysts are finely divided precious metal particles dispersed on ceramic-support materials. However, owing to the agglomeration and growth of the metal particles, those catalysts sometimes reduce the overall surface area available for catalytic conversion, resulting in catalytic activity deterioration. Moreover, almost no reports in the literature have been dedicated to noble metals impregnated in perovskite-type structures. For lanthanum-based perovskite-type A₂BO₄ mixed oxides, there is a synergistic effect through partial substitution of lanthanum by divalent ions, in particular Sr²⁺. Due to the presence of two types of A cations, this causes an increase in their average oxidation state and results in better catalytic performance. The influence on synthesis of partial substitution in the B site using noble metals has been less investigated than the structures and catalytic properties of those mixed oxides. Since the B-site ion is the framework ion, which largely affects the catalytic activity, it is very important to study the relationship between structure and performance of the catalyst

in order to choose better catalytic materials. The work presented in this study is a continuation of the studies performed in our laboratory on LaSrCoO₄ by the ethylene diamine tetraacetic acid (EDTA) complex decomposition method.^{14,15} In this paper, using the amorphous citric acid and EDTA complex decomposition method, a series of catalysts was prepared and characterized. With the reduction of NO by CO as a test reaction, the catalytic performances of all catalysts were investigated. To reveal factors controlling the catalysts' performance, XRD, FTIR, BET and XPS were employed.

2. Experimental

2.1. Preparation of Catalysts

LaSrCo_{0.9}Pd_{0.1}O₄ mixed oxide was prepared by amorphous citric acid and EDTA complex decomposition. In the synthesis, lanthanum nitrate, strontium nitrate, cobalt nitrate, palladium nitrate, EDTA and citric acid (all at AR grade purity) were used. A clear solution of citric acid, EDTA and NH₃/H₂O was prepared and then added to a solution of the metal nitrates of appropriate La, Sr, Co and Pd concentrations, to form the metallic amorphous complexes. The ratio of citric acid:EDTA:total metal ions and pH value were kept at 1.5:1.0:1.0 and 7.0–9.0. With the evaporation of water at 80 °C, a dark gel was formed, and the precursor was obtained after the solution was dried completely at 110 °C. LaSrCo_{0.9}Pd_{0.1}O₄ mixed oxide was prepared by decomposing the precursor in air. At first, the temperature was raised to 500 °C at a slow heating rate (about 8 °C min⁻¹). The sample was kept at this temperature for 100 min to promote the decomposition of organic components. Then, the temperature was increased to 850 °C, and maintained for 8 h to promote the formation of perovskite-type mixed oxide. The mixed oxide was divided into two portions, one portion was reduced in 10 % hydrogen balanced with nitrogen gas at 850 °C for 1 h, which was marked as LaSrCo_{0.9}Pd_{0.1}O₄ (reduced); the other portion was reduced in the same reducing gas at 850 °C for 1 h and then oxidized in

* To whom correspondence should be addressed. E-mail: hua_zh@163.com

air at the same temperature for 1 h, which was marked as $\text{LaSrCo}_{0.9}\text{Pd}_{0.1}\text{O}_4$ (reduced and oxidized). In order to enable intercomparison, LaSrCoO_4 mixed oxide was also prepared by the method in air, which was marked as LaSrCoO_4 (reduced). The sintered pellet was crushed and sieved to *ca.* 0.250 ~ 0.177 mm.

2.2. Characterization Techniques

The XRD analysis was performed using a Bruker D8/ADVANCE X-ray diffractometer (Bruker, Karlsruhe, Germany), with the operation conditions as 40 kV/40 mA, Cu K_α radiation and nickel filter. The step scans were taken over a range of 2θ angles from 20 to 80°.

The FTIR analysis was carried out on a Nicolet AVATAR 370 spectrophotometer (Nicolet, Waltham, MA, USA) with KBr pressed pellets in the wavenumber range of 1000–400 cm^{-1} .

The XPS analysis was carried out on a Perkin-Elmer PHI 5000C ESCA X-ray photoelectron spectrometer (Perkin-Elmer, Waltham, MA, USA) using Al K_α radiation source ($h\nu = 1486.6$ eV). The calcination samples were pressed into small stainless-steel cylinders and outgassed at 10^{-5} Pa for 1 h before they were moved into the analysis chamber. The residual pressure in the ion-pumped analysis chamber was maintained below 1.3×10^{-7} Pa during data acquisition. Pretreatments in hydrogen were carried out at 400 °C. Energy regions of the photoelectrons were scanned at a pass energy of 20 eV. Each spectral region was scanned a number of times to obtain good signal to noise ratios. Peak intensities were estimated by calculating the integrated area of each peak after subtraction of the S-shaped background and fitting to a curve consisting of Lorentzian and Gaussian lines of variable proportions. Although surface charging was observed for all the samples, accurate binding energies (BE) (± 0.2 eV) could be determined by charge reference to the C_{1s} peak at 285.00 eV.

The specific surface areas and pore volumes of the samples were determined by nitrogen physisorption at -196 °C using a Micromeritics ASAP 2000 instrument (Micromeritics Instrument Corp., Norcross, GA, USA). Prior to the adsorption measurements, samples were outgassed at 130 °C.

2.3. Activity Measurements

The catalytic tests for the NO reduction by CO were carried out at atmospheric pressure in an automatic Micromeritics flow reactor with standard feed compositions comprising 5000 ppm NO, CO (5 % v/v) and He (balance) over 80 mg catalyst ($W/F = 0.16$ g s cm^{-3}). The gas composition was analyzed before and after the reaction by on-line gas chromatography with thermal conductor detector (TCD) and connected with a computer integrator system using a TDX-01 (2 m) column (Tianjing, China) for N_2 and CO, and porapak Q (3 m) column for NO, CO_2 and N_2O , respectively. The ambient temperatures for the columns and TCD were 50 °C and 75 °C, respectively. Activity is expressed as conversion of NO to N_2 at fixed experimental conditions:

$$Y_{\text{N}_2} = \frac{2[\text{N}_2]}{[\text{NO}]_{\text{in}}} \times 100 \% \quad (1)$$

$$Y_{\text{N}_2} = X_{\text{NO}} \times S_{\text{N}_2} \quad (2)$$

$$X_{\text{NO}} = \frac{[\text{NO}]_{\text{in}} - [\text{NO}]_{\text{out}}}{[\text{NO}]_{\text{in}}} \times 100 \% \quad (3)$$

$$S_{\text{N}_2} = \frac{2[\text{N}_2]}{[\text{NO}]_{\text{in}} - [\text{NO}]_{\text{out}}} \times 100 \% \quad (4)$$

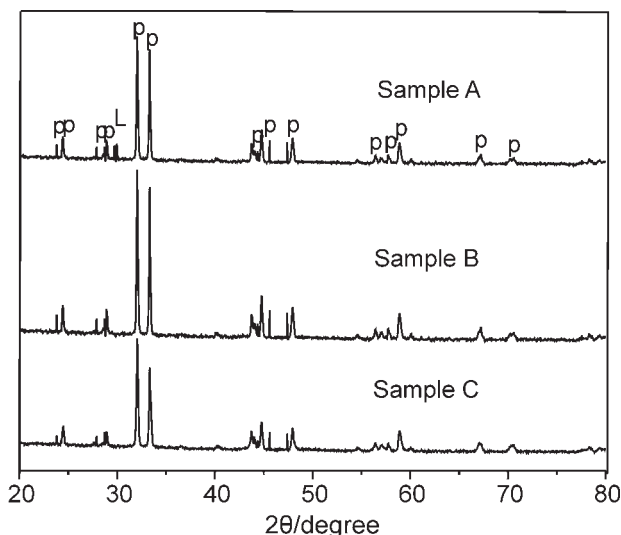


Figure 1 XRD pattern of the mixed oxides. P: perovskite-type LaSrCoO_4 ; L: La_2O_3 .

3. Results and Discussion

3.1. Characterization of Catalysts

The XRD patterns of $\text{LaSrCo}_{0.9}\text{Pd}_{0.1}\text{O}_4$ (reduced), $\text{LaSrCo}_{0.9}\text{Pd}_{0.1}\text{O}_4$ (reduced and oxidized) and LaSrCoO_4 (reduced) are shown in Fig. 1. These patterns clearly reveal characteristic peaks of perovskite-type crystal structure A_2BO_4 , but a metallic Pd signal was not observed by XRD. This can be explained by the fact that the noble metal Pd exists as highly dispersed clusters, or in the amorphous state, or a combination of these two phenomena in $\text{LaSrCo}_{0.9}\text{Pd}_{0.1}\text{O}_4$ (reduced) and $\text{LaSrCo}_{0.9}\text{Pd}_{0.1}\text{O}_4$ (reduced and oxidized). In the case of $\text{LaSrCo}_{0.9}\text{Pd}_{0.1}\text{O}_4$ (reduced and oxidized), the diffraction pattern is rather strong, indicating the presence of perfect crystallites, in accordance with the large pore volume area exhibited in Table 1. The XRD pattern of $\text{LaSrCo}_{0.9}\text{Pd}_{0.1}\text{O}_4$ (reduced), with weak signals of lanthanum oxide, indicates that the destruction of the perovskite-type structure take place gradually during the reduction period.

The FTIR spectra of these three samples in the region 1000–400 cm^{-1} are presented in Fig. 2. All the spectra of the mixed oxides present the most intense bands of the support at *ca.* 500 and 680 cm^{-1} ; the absorption band at *ca.* 500 cm^{-1} is attributed to the stretching vibration of A-O-B of A_2BO_4 belonging to A_{2u} symmetry and the absorption band at *ca.* 680 cm^{-1} belongs to the stretching vibration of B-O₂ bonds in the A_2BO_4 structure.¹⁶ The FTIR spectra of these mixed oxides present weak absorptions at

Table 1 BET surface area, pore volume and catalytic behaviour of the samples.^a

Sample	$\text{LaSrCo}_{0.9}\text{Pd}_{0.1}\text{O}_4$ (reduced)	$\text{LaSrCo}_{0.9}\text{Pd}_{0.1}\text{O}_4$ (reduced and oxidized)	LaSrCoO_4 (reduced)
$S_{\text{BET}}/\text{m}^2 \text{g}^{-1}$	11.4	10.2	8.9
$V_p/\text{cm}^3 \text{g}^{-1}$	0.112	0.148	0.123
$T_{50}/^\circ\text{C}$	258	243	256
$T_{99}/^\circ\text{C}$	346	335	353
RR/ $\text{mmol g}^{-1} \text{h}^{-1}$	2.75	3.42	2.22
SRR/ $\text{mmol m}^{-2} \text{h}^{-1}$	0.241	0.335	0.249

^a S_{BET} : BET surface area; V_p : pore volume; T_{50} , T_{99} : temperature values for 50 and 99 % NO conversion; RR: reaction rate at 300 °C; SRR: surface reaction rate at 300 °C.

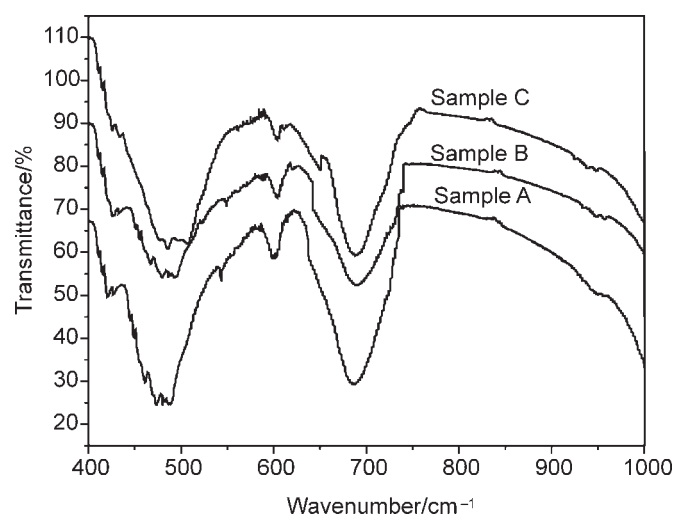


Figure 2 FTIR spectra of the mixed oxides.

640–580 cm^{-1} , which indicates that the structure A_2BO_4 becomes microstrained, but the low density microstrain does not change their original structure. This is in accordance with the XRD results.

The XPS spectra of $\text{Co}_{2p_{3/2}}$ present a main photoelectron peak located at 780.8 eV with a shake-up peak at ca. 793.5 eV for the samples (see Fig. 3). Accompanied by a progressive decrease of the intensity of the shake-up peak, the main photoelectron peak shifts towards lower binding energy for LaSrCoO_4 (reduced) (781.1 eV), $\text{LaSrCo}_{0.9}\text{Pd}_{0.1}\text{O}_4$ (reduced) (780.7 eV), and $\text{LaSrCo}_{0.9}\text{Pd}_{0.1}\text{O}_4$ (reduced and oxidized) (780.5 eV). These three samples suggest the presence of Co^{3+} , in addition to Co^{2+} species, on their surfaces because of the characteristics peak of Co^{2+} and Co^{3+} located at 780.8 or 793.5 eV,¹⁷ and the concentration of Co^{3+} is different for different samples. The chemical state of Pd on the surface of $\text{LaSrCo}_{0.9}\text{Pd}_{0.1}\text{O}_4$ was analyzed by XPS after reduction or reduction-oxidation treatment (see Fig. 3). According to the binding energies of Pd^{n+} and Pd^0 ,¹⁸ the $\text{Pd}_{3d_{5/2}}$ peak in $\text{LaSrCo}_{0.9}\text{Pd}_{0.1}\text{O}_4$ (reduced and oxidized) has a binding energy of Pd^{2+} and an unusual binding energy of Pd^{3+} and/or Pd^{4+} , which shows that cationic Pd is located at the B-site of the perovskite-type crystals as a solid solution and theoretical calculations have also suggested that Pd has the capacity to exist at extraordinarily high oxidation states at the B site.^{19,20} However, for $\text{LaSrCo}_{0.9}\text{Pd}_{0.1}\text{O}_4$ (reduced), the peak due to the Pd-O bond became less intense and that due to the Pd-Pd bond became more intense during reduction, the Pd^{3+} and/or Pd^{4+} peak disappeared, the Pd^{2+} peak declined and a new, low intensity peak of Pd^0 appears. It can be conjectured that a few metallic Pd^0 species segregate out from the perovskite-type framework and are finely dispersed on the catalyst surface, though the XRD pattern does not show diffraction peaks originating from metallic Pd.

3.2. Activity of Catalysts

All samples were tested by reduction of NO by CO. The activity and selectivity profiles as functions of the reaction temperature are presented in Fig. 4, which shows that complete conversion of NO is attained with all samples at temperature below 360 °C and the noble metal Pd evidently displays a strong influence on the catalytic performance. The result of comparing temperature values for 50 and 99 % NO conversion (marked as T_{50} or T_{99}) reported in Table 1 indicates that the best catalytic performance is shown by $\text{LaSrCo}_{0.9}\text{Pd}_{0.1}\text{O}_4$ (reduced and oxidized). $\text{LaSrCo}_{0.9}\text{Pd}_{0.1}\text{O}_4$ (reduced) and LaSrCoO_4 (reduced) have similar

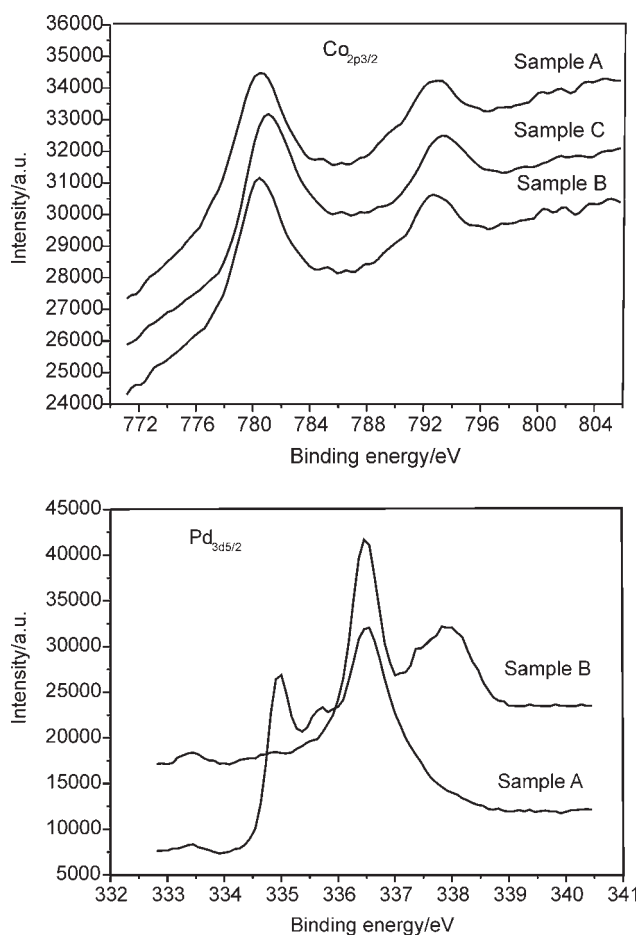


Figure 3 $\text{Co}_{2p_{3/2}}$ and $\text{Pd}_{3d_{5/2}}$ XPS spectra of the mixed oxides.

T_{50} activities, but lower than that of $\text{LaSrCo}_{0.9}\text{Pd}_{0.1}\text{O}_4$ (reduced and oxidized), and their relevant conversion curves intersect at 270 °C, LaSrCoO_4 (reduced) becoming less active than $\text{LaSrCo}_{0.9}\text{Pd}_{0.1}\text{O}_4$ (reduced) above that temperature. The relatively higher catalytic performance exhibited by $\text{LaSrCo}_{0.9}\text{Pd}_{0.1}\text{O}_4$ (reduced) and $\text{LaSrCo}_{0.9}\text{Pd}_{0.1}\text{O}_4$ (reduced and oxidized) is most probably due to the formation of Pd^{n+} in these samples and the fact that it acts as an active state improving the NO reduction by CO, compared with LaSrCoO_4 (reduced). $\text{LaSrCo}_{0.9}\text{Pd}_{0.1}\text{O}_4$ (reduced) has a considerably lower activity than that of $\text{LaSrCo}_{0.9}\text{Pd}_{0.1}\text{O}_4$ (reduced and oxidized) above 220 °C, although equally selective, which can be due to the occurrence of Pd species during reduction.

In addition, since the specific surface area varies from sample to sample (see Table 1), activity is normalized to the specific surface area. The BET surface areas for $\text{LaSrCo}_{0.9}\text{Pd}_{0.1}\text{O}_4$ are much higher than that of the non-palladium LaSrCoO_4 (reduced). The pore volume of $\text{LaSrCo}_{0.9}\text{Pd}_{0.1}\text{O}_4$ (reduced and oxidized) exhibits a value of $0.148 \text{ cm}^3 \text{ g}^{-1}$ and is the largest among those samples, which could be due to Pd in $\text{LaSrCo}_{0.9}\text{Pd}_{0.1}\text{O}_4$ mixed oxide after reduction-oxidation being in a 2+, 3+ and/or 4+ state, resulting in the crystal expanding. The influence of the specific surface area on the activity expressed as the specific rate of NO consumption based on unit catalyst mass is also observed in Table 1 at 300 °C. $\text{LaSrCo}_{0.9}\text{Pd}_{0.1}\text{O}_4$ (reduced and oxidized) exhibited the highest specific rate followed by $\text{LaSrCo}_{0.9}\text{Pd}_{0.1}\text{O}_4$ (reduced) and LaSrCoO_4 (reduced). Moreover, the activity scale per unit surface area shows that $\text{LaSrCo}_{0.9}\text{Pd}_{0.1}\text{O}_4$ (reduced and oxidized) is the most active catalyst, and the order is $\text{LaSrCo}_{0.9}\text{Pd}_{0.1}\text{O}_4$ (reduced and oxidized) > LaSrCoO_4 (reduced) > $\text{LaSrCo}_{0.9}\text{Pd}_{0.1}\text{O}_4$ (reduced). Indeed, $\text{LaSrCo}_{0.9}\text{Pd}_{0.1}\text{O}_4$ (reduced and oxidized) with

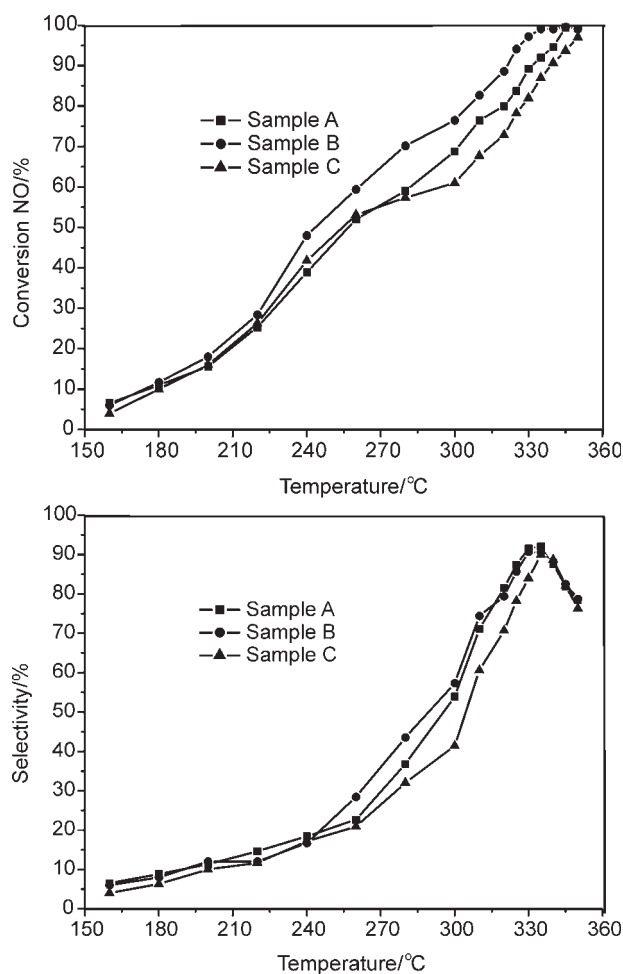


Figure 4 Variation of NO conversion and selectivity with reaction temperature for the NO reduction by CO over the mixed oxides.

the lower surface area shows a surface reaction rate 1.24 times larger than that of $\text{LaSrCo}_{0.9}\text{Pd}_{0.1}\text{O}_4$ (reduced), which indicates that the activity is related not only to the extension of total exposed surface but also to the total number of active sites. Figure 5 shows the strong influence of the temperature and Pd on the intrinsic activity. The maximum of these profiles is $\text{LaSrCo}_{0.9}\text{Pd}_{0.1}\text{O}_4$ (reduced and oxidized) at all temperatures, for which the concentration of active centre at the B site reaches a maximum. Simultaneously, the intrinsic activities of $\text{LaSrCo}_{0.9}\text{Pd}_{0.1}\text{O}_4$ (reduced) and LaSrCoO_4 (reduced) are lower

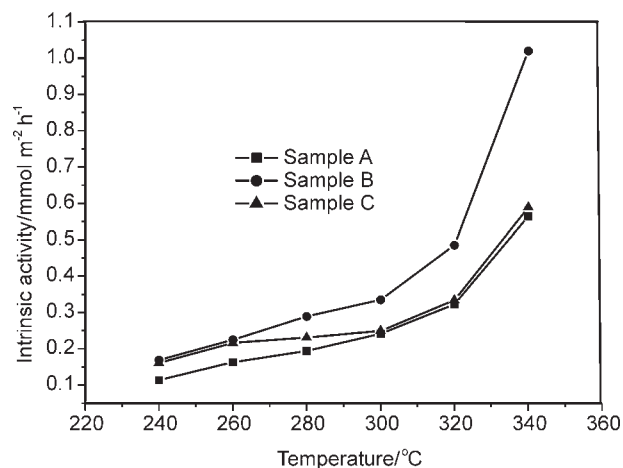


Figure 5 Intrinsic activities of the mixed oxides at reaction temperatures ranging from 240 °C to 340 °C.

than that of $\text{LaSrCo}_{0.9}\text{Pd}_{0.1}\text{O}_4$ (reduced and oxidized), and their relevant intrinsic activity curves are approximately parallel above 300 °C, with $\text{LaSrCo}_{0.9}\text{Pd}_{0.1}\text{O}_4$ (reduced) becoming less intrinsically active than LaSrCoO_4 (reduced) below that temperature. It can also be noted that for these samples activity is different with different methods of preparation.

4. Conclusion

$\text{LaSrCo}_{0.9}\text{Pd}_{0.1}\text{O}_4$ and LaSrCoO_4 were prepared by amorphous citric acid and ethylene diamine tetraacetic acid complex decomposition and tested by the reduction of NO by CO. All samples display characteristic peaks of perovskite-type crystal structure A_2BO_4 . The noble metal Pd has a significant influence on the specific surface areas, pore volumes, binding energies and catalytic properties of the samples. For the NO reduction by CO, catalytic activity shows complete conversion below 360 °C with selectivity to N_2 and the order of activity is $\text{LaSrCo}_{0.9}\text{Pd}_{0.1}\text{O}_4$ (reduced and oxidized) > $\text{LaSrCo}_{0.9}\text{Pd}_{0.1}\text{O}_4$ (reduced) > LaSrCoO_4 (reduced). $\text{LaSrCo}_{0.9}\text{Pd}_{0.1}\text{O}_4$ (reduced and oxidized) exhibits the highest specific rate followed by $\text{LaSrCo}_{0.9}\text{Pd}_{0.1}\text{O}_4$ (reduced) and LaSrCoO_4 (reduced). Moreover, according to the activity scale per unit surface area, $\text{LaSrCo}_{0.9}\text{Pd}_{0.1}\text{O}_4$ (reduced and oxidized) is the most active catalyst, and the order is $\text{LaSrCo}_{0.9}\text{Pd}_{0.1}\text{O}_4$ (reduced and oxidized) > LaSrCoO_4 (reduced) > $\text{LaSrCo}_{0.9}\text{Pd}_{0.1}\text{O}_4$ (reduced).

Acknowledgements

The work described above was supported by Jianggangshan University and by the Education Bureau of Jiangxi, China (Project No. GJJ09339) and the Science and Technology Program of Jianggangshan University (Grant No. JZ0730).

References

- 1 N. Guillaume, S.D. Peter and M. Primet, *Appl. Catal. B*, 1996, **10**, 325–330.
- 2 R.J.H. Voorhoeve, J. P. Remeika, L.E. Trimble, A.S. Cooper, E.J. Disalvo and P.K. Gallagher, *J. Solid State Chem.*, 1975, **14**, 395–406.
- 3 D. Ferri, L. Forni, M.A.P. Dekkers and B.E. Nieuwenhuys, *Appl. Catal. B*, 1998, **16**, 339–345.
- 4 Y. Yokoi and H. Uchida, *Catal. Today*, 1998, **42**, 167–174.
- 5 J.M.D. Tascon, L.G. Tejuca and C.H. Rochester, *J. Catal.*, 1985, **95**, 558–566.
- 6 H. Kishimoto, N. Sakai, T. Horita, K. Yamaji, M.E. Brito and H. Yokokawa, *Solid State Ionics*, 2008, **179**, 1338–1342.
- 7 Y. Teraoka, H. Nii, S. Kagawa, K. Jansson and M. Nygren, *Chem. Lett.*, 1996, **6**, 323–324.
- 8 Y. Teraoka, H. Nii, S. Kagawa, K. Jansson and M. Nygren, *J. Mat. Chem.*, 1996, **6**, 97–102.
- 9 S.D. Peter, E. Garbowski, N. Guillaume, V. Perrichon and M. Primet, *Catal. Lett.*, 1998, **54**, 79–84.
- 10 H. Zhong, X.R. Zeng, L.T. Luo and D.S. Liu, *React. Kinet. Catal. Lett.*, 2005, **87**, 139–148.
- 11 X.M. Yang, L.T. Luo and H. Zhong, *Appl. Catal. A*, 2004, **272**, 299–303.
- 12 L.T. Luo, H. Zhong and X. M. Yang, *J. Serb. Chem. Soc.*, 2004, **69**, 783–790.
- 13 X. M. Yang, L.T. Luo and H. Zhong, *React. Kinet. Catal. Lett.*, 2004, **81**, 219–227.
- 14 X. M. Yang, L.T. Luo and H. Zhong, *Catal. Commun.*, 2005, **6**, 13–17.
- 15 H. Zhong and X.R. Zeng, *J. Serb. Chem. Soc.*, 2006, **71**, 685–693.
- 16 P. Odier and M. Leblank, *Mater. Res. Bull.*, 1986, **21**, 787–802.
- 17 Y. Olamoto and T. Imanaka, *Appl. Catal. B*, 1991, **73**, 249–254.
- 18 J.F. Moulder, W.F. Stickle, P.E. Sobol and K.D. Bomben, *Handbook of X-Ray Photoelectron Spectroscopy*, Perkin-Elmer, Waltham, MA, USA, 1992.
- 19 H. Tanaka, I. Tan, M. Uenishi, M. Kimura and K. Dohmae, *Top. Catal.*, 2001, **16/17**, 63–70.
- 20 D. Ganguli, *J. Solid State Chem.*, 1979, **30**, 353–356.